ACS Energy Letters

Cite This: ACS Energy Lett. 2017, 2, 2647-2652 http://pubs.acs.org/journal/aelccp

LETTER

Slow Cooling of Hot Polarons in Halide Perovskite Solar Cells

Jarvist Moore Frost,*[,†,‡] Lucy D. Whalley,[†] and Aron Walsh*[,†,¶]

[†]Department of Materials, Imperial College London, Exhibition Road, London SW7 2AZ, United Kingdom

[‡]Centre for Sustainable Chemical Technologies and Department of Chemistry, University of Bath, Claverton Down, Bath BA2 7AY, United Kingdom

[¶]Department of Materials Science and Engineering, Yonsei University, Seoul 03722, Korea

Supporting Information

ABSTRACT: **Halide perovskites show unusual thermalization kinetics for above-bandgap photoexcitation. We explain this as a consequence of excess energy being deposited into discrete large polaron states. The crossover between low-fluence and high-fluence "phonon bottleneck" cooling is due to a Mott transition where the polarons overlap ($n \geq 10^{18}$ cm^{-3}) and the phonon subpopulations are shared. We calculate the initial rate of cooling (thermalization) from the scattering time in the Fröhlich polaron model to be 78 meV ps^{-1} for $CH_3NH_3PbI_3$. This rapid initial thermalization involves heat transfer into optical phonon modes coupled by a polar dielectric interaction. Further cooling to equilibrium over hundreds of picoseconds is limited by the ultralow thermal conductivity of the perovskite lattice.**

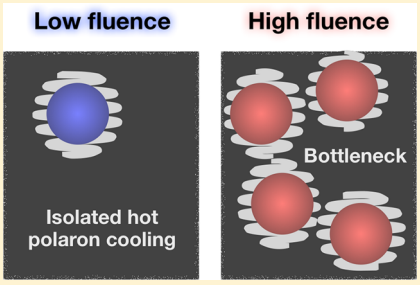

A key challenge in the device physics of photovoltaic materials is understanding where the above-bandgap photon energy goes and how to control it. Thermalization of "hot" (above bandgap) carriers is normally a fast femtosecond process in pure crystals. It is a loss process in photovoltaics and is a major factor underpinning the Shockley–Queisser limit for power conversion efficiencies.[1] To avoid this loss pathway, hypothetical device architectures have been devised by which these hot carriers can be extracted.[2] A fundamental material limit is how *far* the carriers move in the active photovoltaic layer before cooling to thermal equilibrium.

There is growing literature on the kinetics of carrier cooling in halide perovskites.[3−9] The behavior has been linked to a "phonon bottleneck" at high fluence and more generally to the formation and stability of polaronic charge carriers. In addition, it has been established that halide perovskites exhibit low thermal conductivity, which could be affecting the photophysical processes. Thermal conduction in methylammonium lead iodide ($CH_3NH_3PbI_3$ or MAPI) is almost as low as that for a solid-state material can be—the material forms a phonon glass.[10−12]

In this Letter, we consider the microscopic thermal processes in halide perovskite solar cells underpinning the formation, thermalization, and cooling of charge carriers photogenerated from above-bandgap illumination. We describe how the formation of hot electron and hole charge carriers in the form of Fröhlich polarons resonates with a subpopulation of phonon states (thermalization of 78 meV ps^{-1}). These then cool slowly (over hundreds of ps) due to low thermal conductivity resulting from short phonon lifetimes. We further show that $CsPbI_3$ has a larger thermal conductivity than $CH_3NH_3PbI_3$, which accelerates the kinetics of hot carrier cooling.

Measurements and Models of Carrier Cooling. Relative to the light intensity generated by a laboratory laser, the sun is dim. The charge density maintained by steady-state generation, recombination, and extraction of photogenerated charges under solar irradiation is estimated to be 10^{15} cm^{-3}.[13] Careful control of signal-to-noise is required to reach this low-fluence regime in transient studies. The photophysics at higher fluence can be very different from an operating device under sunlight.

As well as fluence, there is flexibility in what excitation energy to pump at. In a two-band effective mass model, excitation above the bandgap results in proportionally higher energy electrons and holes. However, lead halide perovskites have multiple optically accessible bands. Spin−orbit coupling splits the Pb 6p conduction band into levels calculated (by quasiparticle GW theory) at +1.6 and +3.1 eV above the valence band maximum.[14] These values neglect two-particle (excitonic) effects and electron−phonon renormalization. The second transition is observed by spectroscopic ellipsometry as a critical point at 2.5 eV.[15] Exciting well below the experimentally observed second critical point at 2.5 eV is required to generate a population of hot carriers in the first conduction band.

Received: September 12, 2017
Accepted: October 23, 2017
Published: October 23, 2017

DOI: 10.1021/acsenergylett.7b00862
ACS Energy Lett. 2017, 2, 2647−2652

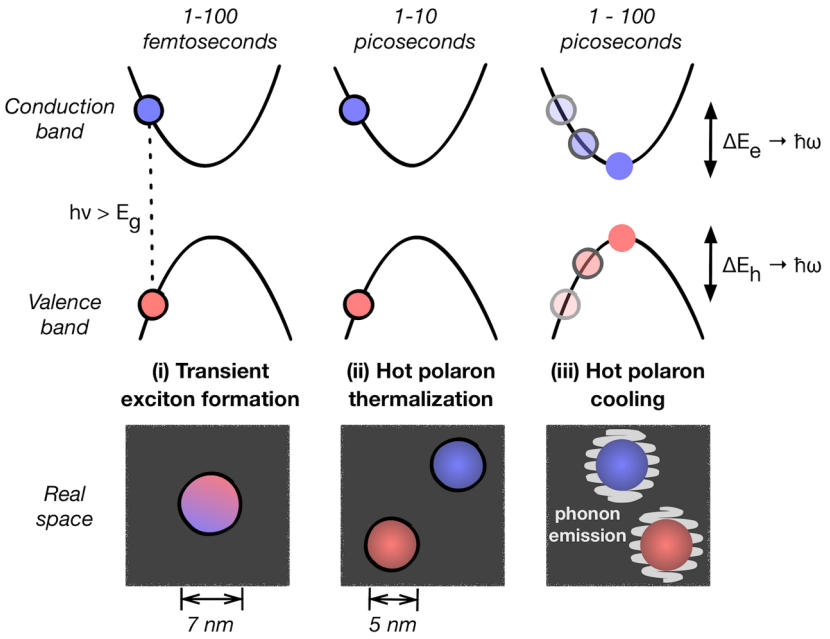

Figure 1. Physical processes involved during the photogeneration of charge carriers, which results from above-bandgap illumination in a halide perovskite: (i) transient exciton generation; (ii) exciton dissociation, hot polaron formation, and thermalization; (iii) hot phonon relaxation to the band edge limited by the lattice thermal conductivity. Note that we make a distinction between *thermalization*, which we define as equilibration with local phonon modes, and *cooling*, which is equilibration with the extended bulk solid. Together, they form the hot carrier relaxation process.

The common experimental choice of 400 nm (3.1 eV) excitation is problematic in terms of interpreting the data. We estimate from the partial optical density of states (see ref 15 Figure 4c) that between 10 and 20% of the excitation flux at 3.1 eV goes into the higher conduction band. This confuses the analysis as a combination of (delayed) band-to-band transitions will overlap with the hot carrier cooling.

There is evidence[3,4,7] that at high fluence ($n \geq 10^{18}$ cm^{-3}), cooling of above-bandgap photogenerated charges in MAPI is slow ($\tau \approx 100$ ps). This has been ascribed to a "phonon bottleneck"[16] effect. Yang et al.[7] recently studied this high-fluence cooling regime in some detail and proposed a link between the phonon bottleneck and low thermal conductivity. The existence of a phonon bottleneck even in conventional inorganic quantum dots is controversial[17] and requires weak coupling to the fast dissipating (speed of sound) acoustic vibrational modes.

A recent transient absorption microscopy study of polycrystalline MAPI suggests ballistic transport of the slowly cooling carriers generated by excitation at 3.14 eV.[9] Similarly, a combined transient absorption and time-resolved photoluminescence study on MAPI[8] found unusual transient behavior when pumping at 3.1 eV. They see a direct "cooling", which they associate with a large momentum transition (i.e., an optical phonon mode) between the Brillouin zone boundary and zone center. These unusual data may in part be due to transitions involving higher conduction bands.

Zhu et al.[6] studied the bromine analogue, pumping at modest fluence (~7×10^{16} cm^{-3}), ~700 meV above the bandgap. No "hot" emission is observed in transient photoluminescence for the inorganic cesium material, whereas the organic–inorganic materials possess an addition high-energy emission decaying with a time constant of 160 ps.

Kawait et al.[18] calculated carrier cooling from first-principles via electron–phonon interactions for $CsPbI_3$ and bare PbI_3^- octahedra (with a homogeneous background charge to maintain charge neutrality). However, the neglect of spin–orbit coupling to calculate the electronic structure calls the energy dissipation rate into question as the conduction band (Pb 6p) energy, dispersion, and degeneracy are significantly altered. The electron–phonon coupling was calculated assuming harmonic vibrations and thus may further miss the major contribution in highly anharmonic systems such as the halide perovskites.

All of the transient spectroscopic studies reported so far suggest that a hot photoexcited state persists in hybrid halide perovskites with a characteristic cooling time of up to 100 ps. There are three dynamic processes that we need to understand: (1) The photon will first be absorbed into a particular volume of the material (the exciton, a transient Coulomb bound electron–hole pair); (2) the exciton will then separate into hot carriers (electron and hole polarons), which will thermalize with a local (polar) phonon population; (3) the polaron phonon cloud will equilibrate by the transfer of thermal energy to the lattice, leading to a cooled charge carrier state. These processes are illustrated in Figure 1. Each of these states can be modeled with different levels of theory, from the microscopic to the mean-field. We will first discuss them individually and then assess the full process.

Transient Wannier Exciton Formation. Whether (three-dimensional) lead iodide perovskites support an equilibrium population of excitons (bound electron–hole pairs) is a matter of some experimental debate. Absorption-based measurements typically indicate the existence of an exciton state below the bandgap,[19] whereas there is no evidence in emission. We explain this disagreement as being due to the time scale for the measurements. Absorption probes transient states, whereas emission is sensitive to a steady state of electrons and holes. The difference between the optical dielectric constant ($\epsilon_\infty \approx 5$, response on a time scale of femtoseconds) and the larger static

DOI: 10.1021/acsenergylett.7b00862
ACS Energy Lett. 2017, 2, 2647–2652

dielectric constant (ϵ_0 > 20, response on a time scale of picoseconds) means that the exciton is transiently stabilized by the optical dielectric constant.

Prediction of the exciton state is a challenge for first-principles electronic structure theory. Solution of the Bethe–Salpeter equation (which contains the first-order contribution to electron–hole binding) is computationally demanding and more so to achieve convergence. The resulting binding energy only considers the response of electronic excitations (i.e., ϵ_∞). The work of Bokdam et al.[20] gives a value for MAPI of 45 meV.

An effective mass model of Wannier excitons[21] considers the photoexcited electron and hole to individually be polarons. The interaction is a statically screened Coulomb interaction of the bare charges. This forms a hydrogenic bound state within the nearly free-electron environment provided by the band effective masses. Simplifying to a single-particle system with a reduced effective mass, this is solved exactly to give a spectrum

$$E_n(k) = -\frac{\mu q^4}{2\hbar^2\epsilon^2 n^2} + \frac{\hbar^2 k^2}{2(m_e + m_h)} \quad (1)$$

Here, $E_n(k)$ is the energy of state n, with k as the crystallographic momentum. ϵ is the dielectric constant; $\mu = m_e m_h/(m_e + m_h)$ is the reduced carrier mass; q is the electron charge; and $\hbar$ is the reduced Planck constant.

For the ground state of the exciton relative to separated charges, n = 1 and k = 0 (Γ point). The associated exciton radius (analogous to a Bohr radius) is defined as

$$a_\mu = \frac{\epsilon\hbar^2}{\mu q^2} \quad (2)$$

Our calculations were cross-checked against CdS.[22]

The short time scale (100 fs) exciton is stabilized by the optical dielectric constant. With values (by QSGW[23]) of ϵ = 4.5, m_e = 0.12, and m_h = 0.15, the exciton binding energy is 44.8mev with a Bohr radius of a_μ = 35.7 Å. Once the full dielectric response of the lattice occurs (ϵ = 24.1), the binding energy reduces to 4 meV, and the exciton orbital expands to an enormous size; the exciton has separated. On the time scale of the atomic motion (picoseconds) giving rise to the static dielectric constant, the exciton decomposes into separate electron and hole polarons. The initial hot exciton is transient. This model agrees well with a recent study[24] that measured the exciton binding energy as 13.5 meV and the associated dephasing time (which we consider to be the exciton separation) of 1 ps.

Large Polaron Formation. A polaron quasi-particle consists of a charge carrier (electron or hole) wave function that has been localized in a dynamically generated potential due to the polar response of the lattice, which can be described within the Fröhlich model. The calculated polaron coupling constants α = 2.4 (electron) and 2.7 (hole) fall in the intermediate coupling regime (defined as 1 < α < 6).[25] Quantifying the size of a polaron is difficult, but estimates can be made within the Fröhlich model (see details in the Supporting Information). The polaron decreases in size as a function of temperature (Figure 2), with large polaron radii of 26.8 (electron) and 25.3 Å (hole) calculated at 300 K. Within the same model, we predict a broad polaron absorption feature (2.25–6.75 THz), a Franck–Condon resonance at 186 meV (45 THz), and coherent exchange of energy between the electron and phonon (on a time scale between these limits). Further details on these estimates are presented in the Supporting Information.

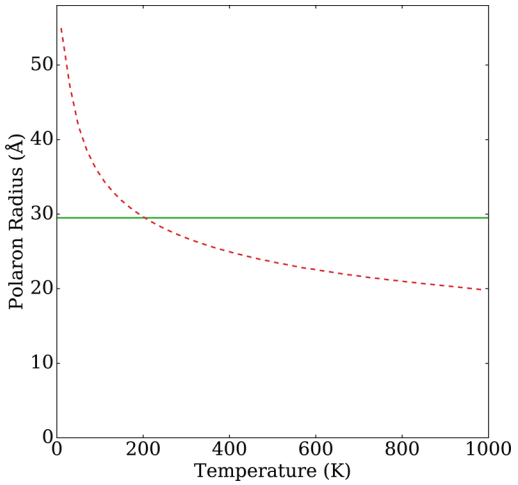

Figure 2. (Red dashed line) Temperature-dependent electron (m_e = 0.12) polaron radius (Å) calculated from a numerical solution to the Fröhlich polaron model. (Horizontal solid green line) Polaron radius from the common (athermal) small-α approximation.

With a polaron radius, we can now estimate at what excitation density the polarons overlap. If we define overlap as when the polarons "touch" (i.e., each occupies a cube with the sides twice the radius) and include a factor of 2 for capturing both hole and electron polarons, the density is simply

$$\rho = V^{-1} = (2(2r_f)^3)^{-1} \quad (3)$$

Expressed in standard units, the critical carrier density is 3 × 10^{18} cm^{-3}. This result provides a simple and direct explanation for the high-fluence transition to where the carrier cooling is limited by a bottleneck.[3,4] Namely, the polarons are overlapping to the extent that the above-bandgap thermal energy is shared between overlapping polaron states and cannot dissipate. In semiconductor physics, this is a Mott semiconductor–metal transition. The phenomenological Mott criterion[26] for polaron overlap predicts a density of 4 × 10^{17} cm^{-3}. These estimates also provide a real-space explanation of the observed lasing threshold of 10^{18} cm^{-3} in that the electron and hole wave functions are forced into an overlapping (and therefore optically active) configuration.

Hot Polaron States. We have established that the size of the transient exciton is commensurate with the polaron state. We expect the exciton to quickly (on a time scale of picoseconds) decompose into polarons. As the bare-band effective masses in halide perovskites are nearly balanced, the hole and electron polarons are similar in character and size. Without a more detailed physical picture of the process, we assume an equipartition of the above-bandgap energy ($h\nu$ > 1.6 eV for MAPI) into the hot hole and electron polaron states. Considering excitations up into the near-UV at 4.0 eV, the initial polaron energy could be as high as 1.2 eV.

An excess carrier energy of 1.2 eV is translated by $E = k_B T$ to a single degree-of-freedom "electron temperature" of 13900 K. A way of interpreting the high temperatures extracted from transient experiments is to invert this identity and calculate among how many microscopic states the excess energy has so far been shared. This way, an estimate is made of the size of the thermal bath, the subpopulation of states coupled to the hot carrier. Once fully thermalized (local equipartition), this energy will be shared among all accessible phonon states within the polaron. In a continuum model, the eventual (fully

DOI: 10.1021/acsenergylett.7b00862
ACS Energy Lett. 2017, 2, 2647–2652

thermalized) polaron temperature depends on the volume and specific heat capacity (C_V) of the polaron. This we can calculate from the phonon density of states. Summing over the Bose–Einstein occupied phonon modes for MAPI, we find a per-unit cell specific heat capacity of 1.25 meVK^{-1} at 300 K. The wavefunction of an electron polaron of radius 26.8 Å occupies over 300 unit cells of the crystal. The maximum initial temperature from considering the above-bandgap energy (1.2 eV) being distributed thermodynamically across the inorganic phonon modes associated with the phonon unit cells is 3 K. This temperature seems too small to explain the low-fluence hot carrier results. Instead, some mechanism to cause greater confinement, or a reduced effective specific heat capacity, must be invoked.

The polaron radius that we have calculated is an upper bound: bulk polaron states are further localized by disorder.[27] The temperature increases with localization ($T \propto r^{-3}$), as shown in Figure 3. Point and extended defects (surfaces, interfaces, dislocations, grain boundaries) may localize polarons further and therefore be exposed to local heating and degradation of the halide perovskite material.

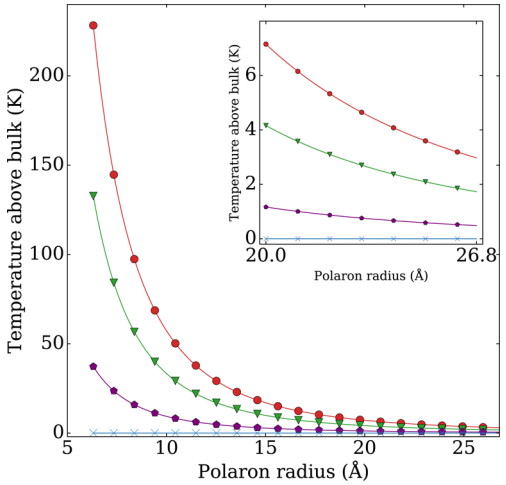

Figure 3. Thermalized polaron temperature in MAPI as a function of polaron radius and excitation energy (red circles = 4 eV, green triangle = 3 eV, purple pentagon = 2 eV, blue cross = 1.61 eV) assuming a bulk value of the heat capacity. The calculated bulk electron polaron radius of 26.8 Å provides an upper bound for polaron size. We take the lattice parameter (6.3 Å) as a lower bound; below this, the continuum large polaron approach is not valid. We consider excitation from the bandgap to near-UV. The inset shows details at larger radii.

Carrier Cooling: Initial Thermalization. The same force driving polaron formation in MAPI, the dipolar electron–phonon interaction, will dominate the initial hot carrier thermalization as zone center optical phonons are generated. The calculated optical phonon inelastic scattering time is τ = 0.12 ps at 300 K.[28] The characteristic optical phonon frequency for MAPI is 2.25 THz,[28] making a quanta ($E = \hbar\omega$) of this vibration equal to 9.3 meV. The thermalization rate by optical phonon emission from the polaron is thus $\frac{\hbar\omega}{\tau}$ = 77.5 meVps^{-1}. This provides an estimate of initial polaron thermalization.

Energy exchange will proceed until the charge carrier is in thermal equilibrium with the subpopulation of coupled phonons. This subpopulation will consist of the zone center (infrared-active) phonon modes in the near vicinity of the polaron. The small size of this population means that the effective specific heat capacity is reduced and a higher effective polaron temperature will be reached compared to that predicted from bulk values. This occurs on a quantized (per photon) basis due to the small set of coupled phonon states in the polaron. This model describes the dilute limit of noninteracting polarons; therefore, there is no dependence on excitation intensity.

Carrier Cooling: Heat Transfer to the Lattice. Similar to electrical conductivity, phonon conductivity is limited by scattering events. In the bulk, the most frequent is phonon–phonon scattering. Due to energy and momentum conservation rules, three-phonon scattering is the lowest-order process. We previously[12] calculated the three-phonon interaction strengths for MAPI and found them to be orders of magnitude stronger than those for CdTe and GaAs. These interactions provide the rates for a stochastic (master equation) representation of how energy flows microscopically toward equilibrium. Direct propagation of this equation with time would provide a microscopic picture of how the subpopulation of phonon states in a polaron scatter and cool.

Here we consider the bulk effect of phonon–phonon scattering. The sum of modal contributions, accounting for the phonon lifetime, group velocity, and heat capacity, gives the overall thermal conductivity.[29] In MAPI, the bulk thermal conductivity from a solution of the Boltzmann transport equation (in the relaxation time approximation) is extremely low, 0.05 W m^{-1} K^{-1} at 300 K.[12] In contrast, the calculated conductivities for GaAs and CdTe are 38 and 9 W m^{-1} K^{-1}, respectively.

To assess the role of the organic cation, a thermal conductivity calculation was made on $CsPbI_3$ in the cubic perovskite phase. Due to the high (O_h) symmetry, the computational cost is greatly reduced when compared to lower-symmetry hybrid halide structures. A complication is that the vibrational instability of the cubic $CsPbI_3$ structure results in a branch of modes having an imaginary frequency, which is not considered in the Brillouin zone summations. In reality, the room-temperature structure of many perovskites is dynamically cubic,[30,31] and such higher-order anharmonicity is not considered here. The calculated thermal conductivity for $CsPbI_3$ is 0.5 W m^{-1} K^{-1} at 300 K. While still low, it is an order of magnitude greater than 0.05 W m^{-1} K^{-1} for MAPI. Kovalsky et al.[32] recently measured thermal conductivity in $CsPbI_3$ as 0.45 W m^{-1} K^{-1} and in MAPI as 0.3 W m^{-1} K^{-1}, with the differences attributed to rotations of $CH_3NH_3^+$. Additional contributions from electron and ion heat transport and issues with sample purity may explain some disparity between theory and experiment.

We first consider bulk heat diffusion in the low-fluence limit. Individual photon quanta are absorbed into isolated hot polarons, cooling by scattering into phonon modes, which then diffuse away from the polaron. Modeling this classically, we can consider the polaron as a hot sphere in a continuum of ambient-temperature material. This reduces to a one-dimensional problem, where the exponent is weighted by the r^2 increasing shell of available states over the surface of the sphere. The initial "top hat" heat distribution is convolved with a Gaussian kernel to give an analytical expression for the evolution of hot carrier energy with time (shown in Figure 4). The rate of cooling is determined by the diffusivity (D)

DOI: 10.1021/acsenergylett.7b00862
ACS Energy Lett. 2017, 2, 2647–2652

$$D = \frac{\kappa}{\rho c_p} \quad (4)$$

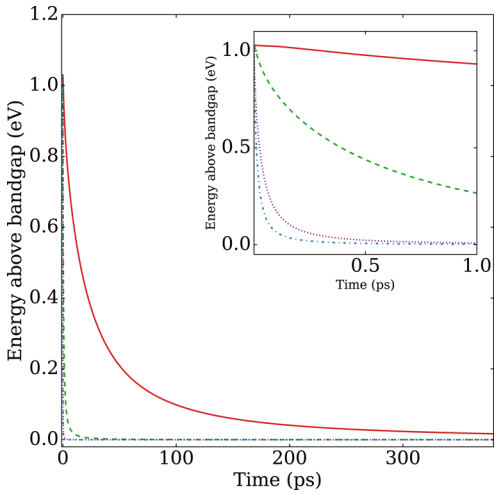

Figure 4. (Red solid line) Energy of a large polaron state (starting at 1.2 eV above the conduction band minimum, with a polaron radius of 26.8 Å) in $CH_3NH_3PbI_3$ as a function of time. The slow rate is due to low thermal conductivity in MAPI (κ = 0.05 W m^{-1} K^{-1}). For comparison, we show the behavior using the thermal conductivities of CdTe (κ = 9, purple dotted line) and GaAs (κ = 38, blue dotted−dashed line). Heat diffuses from MAPI on the order of 100 ps, while for other conductivities, the process is much faster, on the order of 100 fs. This is in agreement with reported experimental values: ref 33 (MAPI) ref 34 (CdTe), and ref 35 (GaAs). Note that at short time scales, measurements of hot carrier cooling in MAPI and $CsPbI_3$(κ = 0.5, green dashed line) may appear linear due to the slower exponential decay. The inset shows a magnification of faster processes around 0−1 ps.

where κ is the thermal conductivity, ρ is the density, and c_p is the specific heat capacity. Phonon−phonon cooling in MAPI is on the order of 100 ps. This compares well to the observed time scale of slow carrier cooling. In $CsPbI_3$, a higher thermal conductivity results in polaron cooling within picoseconds. This is faster than might be expected by naïve consideration of the diffusivity, due to the $D^{3/2}$ scaling of heat conduction from a point in three dimensions.

The phonon bottleneck is associated with a diminished subpopulation of phonon states, originally envisaged in the gapped density of states present in low-dimensional structures.[16] A reduced population of vibrational states strongly couples to the charge carrier in the polaron state. These are the infrared-active phonon modes, identified in lattice dynamic studies[36] as octahedral distortion modes of the PbI_3^- framework. Such distortions for illuminated MAPI have been observed using a time-dependent local structure analysis,[37] and further signatures of polaron formation are observed in the bromide compound.[38]

At low fluence, the subpopulation of polaron phonon modes will thermalize the photoexcited charge carrier to a higher effective temperature than the lattice. The strong phonon−phonon scattering introduces a 100 ps time constant for the bulk flow of thermal energy out of an isolated polaron, which broadly agrees with the observed time constants. Additionally, at high fluence, the polaron states overlap; therefore, diffusion of phonons away from the polaron simply results in reheating other polarons. There is no thermal gradient to drive diffusion. In both cases, eventual cooling will proceed by scattering into other (non-electron−phonon-coupled) phonon modes.

In summary, we have shown how effective mass theories of excitons and polarons—informed by first-principles calculations—can be combined to describe the physical processes behind the slow hot carrier cooling rates observed for halide perovskites. From an interpretation of the density at which the polarons start to overlap, we indicate that significant changes in the photophysics should occur when $n \geq 10^{18}$ cm^{-3}. This corresponds to the observed transition region between low-fluence "high-energy photoluminescence" and high-fluence "hot-phonon bottleneck" regimes.[8] We have underlined the unusual electronic structure of hybrid halide perovskites possessing a second conduction band at +2.5 eV above the valence band and, therefore, caution careful interpretation of photophysics data when pumping with photon energies > 2.5 eV. Finally, we calculated a higher thermal conductivity in the inorganic pervoskite compared to the organic cation hybrid perovskite. This can help explain the lack of hot carrier photoluminescence in the Cs-based material[6] and emphasizes the phonon scattering "rattler" role of the organic cation in limiting thermal dissipation of hot carrier energy.

■ ASSOCIATED CONTENT

Supporting Information

The Supporting Information is available free of charge on the ACS Publications website at DOI: 10.1021/acsenergylett.7b00862.

Detailed theory of large polaron formation and excited states (PDF)

■ AUTHOR INFORMATION

Corresponding Authors

*E-mail: jarvist.frost@imperial.ac.uk (J.M.F.).
*E-mail: a.walsh@imperial.ac.uk (A.W.).

ORCID

Jarvist Moore Frost: 0000-0003-1938-4430
Aron Walsh: 0000-0001-5460-7033

Notes

The authors declare no competing financial interest.
Data files and Jupyter notebooks outlining the calculation steps are available as a repository on GitHub at https://github.com/WMD-group/hot-carrier-cooling.

■ ACKNOWLEDGMENTS

We thank Jonathan M. Skelton for discussions concerning the thermal conductivity calculations. Via our membership of the UK's HEC Materials Chemistry Consortium, which is funded by EPSRC (EP/L000202), this work used the ARCHER UK National Supercomputing Service (http://www.archer.ac.uk). This work was funded by the EPSRC (Grant Numbers EP/L01551X/1, EP/L000202, and EP/K016288/1), the Royal Society, and the ERC (Grant No. 277757).

■ REFERENCES

(1) Shockley, W.; Queisser, H. J. Detailed Balance Limit of Efficiency of p-n Junction Solar Cells. *J. Appl. Phys.* **1961**, *32*, 510−519.
(2) Green, M. A.; Bremner, S. P. Energy Conversion Approaches and Materials for High-Efficiency Photovoltaics. *Nat. Mater.* **2016**, *16*, 23−34.
(3) Price, M. B.; Butkus, J.; Jellicoe, T. C.; Sadhanala, A.; Briane, A.; Halpert, J. E.; Broch, K.; Hodgkiss, J. M.; Friend, R. H.; Deschler, F.

DOI: 10.1021/acsenergylett.7b00862
ACS Energy Lett. 2017, 2, 2647−2652

Hot-Carrier Cooling and Photoinduced Refractive Index Changes in Organic−Inorganic Lead Halide Perovskites. *Nat. Commun.* **2015**, *6*, 8420.
(4) Yang, Y.; Ostrowski, D. P.; France, R. M.; Zhu, K.; van de Lagemaat, J.; Luther, J. M.; Beard, M. C. Observation of a Hot-Phonon Bottleneck in Lead-Iodide Perovskites. *Nat. Photonics* **2016**, *10*, 53−59.
(5) Niesner, D.; Zhu, H.; Miyata, K.; Joshi, P. P.; Evans, T. J. S.; Kudisch, B. J.; Trinh, M. T.; Marks, M.; Zhu, X.-Y. Persistent Energetic Electrons in Methylammonium Lead Iodide Perovskite Thin Films. *J. Am. Chem. Soc.* **2016**, *138*, 15717−15726.
(6) Zhu, H.; Miyata, K.; Fu, Y.; Wang, J.; Joshi, P. P.; Niesner, D.; Williams, K. W.; Jin, S.; Zhu, X.-Y. Screening in Crystalline Liquids Protects Energetic Carriers in Hybrid Perovskites. *Science* **2016**, *353*, 1409−1413.
(7) Yang, J.; et al. Acoustic-Optical Phonon Up-Conversion and Hot-Phonon Bottleneck in Lead-Halide Perovskites. *Nat. Commun.* **2017**, *8*, 14120.
(8) Bretschneider, S. A.; Laquai, F.; Bonn, M. Trap-Free Hot Carrier Relaxation in Lead−Halide Perovskite Films. *J. Phys. Chem. C* **2017**, *121*, 11201−11206.
(9) Guo, Z.; Wan, Y.; Yang, M.; Snaider, J.; Zhu, K.; Huang, L. Long-Range Hot-Carrier Transport in Hybrid Perovskites Visualized by Ultrafast Microscopy. *Science* **2017**, *356*, 59−62.
(10) Pisoni, A.; Jaćimović, J.; Barišić, O. S.; Spina, M.; Gaál, R.; Forró, L.; Horváth, E. Ultra-Low Thermal Conductivity in Organic−Inorganic Hybrid Perovskite $CH_3NH_3PbI_3$. *J. Phys. Chem. Lett.* **2014**, *5*, 2488−2492.
(11) Wang, M.; Lin, S. Anisotropic and Ultralow Phonon Thermal Transport in Organic−inorganic Hybrid Perovskites: Atomistic Insights into Solar Cell Thermal Management and Thermoelectric Energy Conversion Efficiency. *Adv. Funct. Mater.* **2016**, *26*, 5297−5306.
(12) Whalley, L. D.; Skelton, J. M.; Frost, J. M.; Walsh, A. Phonon Anharmonicity, Lifetimes, and Thermal Transport in $CH_3NH_3PbI_3$ from Many-Body Perturbation Theory. *Phys. Rev. B: Condens. Matter Mater. Phys.* **2016**, *94*, 220301.
(13) Johnston, M. B.; Herz, L. M. Hybrid Perovskites for Photovoltaics: Charge-Carrier Recombination, Diffusion, and Radiative Efficiencies. *Acc. Chem. Res.* **2016**, *49*, 146−154.
(14) Frost, J. M.; Azarhoosh, P.; McKechnie, S.; van Schilfgaarde, M.; Walsh, A. A Photon Ratchet Route to High-Efficiency Hybrid Halide Perovskite Intermediate Band Solar Cells. *arXiv:1611.09786 [cond-mat]* **2016** , arXiv: 1611.09786..
(15) Leguy, A. M. A.; Azarhoosh, P.; Alonso, M. I.; Campoy-Quiles, M.; Weber, O. J.; Yao, J.; Bryant, D.; Weller, M. T.; Nelson, J.; Walsh, A.; van Schilfgaarde, M.; Barnes, P. R. F. Experimental and Theoretical Optical Properties of Methylammonium Lead Halide Perovskites. *Nanoscale* **2016**, *8*, 6317−6327.
(16) Bockelmann, U.; Bastard, G. Phonon Scattering and Energy Relaxation in Two-, One-, and Zero-Dimensional Electron Gases. *Phys. Rev. B: Condens. Matter Mater. Phys.* **1990**, *42*, 8947−8951.
(17) Li, X.-Q.; Nakayama, H.; Arakawa, Y. Phonon Bottleneck in Quantum Dots: Role of Lifetime of the Confined Optical Phonons. *Phys. Rev. B: Condens. Matter Mater. Phys.* **1999**, *59*, 5069−5073.
(18) Kawai, H.; Giorgi, G.; Marini, A.; Yamashita, K. The Mechanism of Slow Hot-Hole Cooling in Lead-Iodide Perovskite: First-Principles Calculation on Carrier Lifetime from Electron−Phonon Interaction. *Nano Lett.* **2015**, *15*, 3103−3108.
(19) D'Innocenzo, V.; Grancini, G.; Alcocer, M. J. P.; Kandada, A. R. S.; Stranks, S. D.; Lee, M. M.; Lanzani, G.; Snaith, H. J.; Petrozza, A. Excitons Versus Free Charges in Organo-Lead Tri-Halide Perovskites. *Nat. Commun.* **2014**, *5*, 3586.
(20) Bokdam, M.; Sander, T.; Stroppa, A.; Picozzi, S.; Sarma, D. D.; Franchini, C.; Kresse, G. Role of Polar Phonons in the Photo Excited State of Metal Halide Perovskites. *Sci. Rep.* **2016**, *6*, 28618.
(21) Dresselhaus, G. Effective Mass Approximation for Excitons. *J. Phys. Chem. Solids* **1956**, *1*, 14−22.
(22) Thomas, D. G.; Hopfield, J. J. Exciton Spectrum of Cadmium Sulfide. *Phys. Rev.* **1959**, *116*, 573−582.
(23) Brivio, F.; Butler, K. T.; Walsh, A.; van Schilfgaarde, M. Relativistic Quasiparticle Self-Consistent Electronic Structure of Hybrid Halide Perovskite Photovoltaic Absorbers. *Phys. Rev. B: Condens. Matter Mater. Phys.* **2014**, *89*, 155204.
(24) Luo, L.; Men, L.; Liu, Z.; Mudryk, Y.; Zhao, X.; Yao, Y.; Park, J. M.; Shinar, R.; Shinar, J.; Ho, K.-M.; Perakis, I. E.; Vela, J.; Wang, J. Ultrafast Terahertz Snapshots of Excitonic Rydberg States and Electronic Coherence in an Organometal Halide Perovskite. *Nat. Commun.* **2017**, *8*, 15565.
(25) Stoneham, A. M. *Theory of Defects in Solids*; Oxford University Press, 2001.
(26) Edwards, P. P.; Sienko, M. J. Universality Aspects of the Metal-Nonmetal Transition in Condensed Media. *Phys. Rev. B: Condens. Matter Mater. Phys.* **1978**, *17*, 2575−2581.
(27) Grein, C. H.; John, S. Polaronic Band Tails in Disordered Solids: Combined Effects of Static Randomness and Electron-Phonon Interactions. *Phys. Rev. B: Condens. Matter Mater. Phys.* **1987**, *36*, 7457−7468.
(28) Frost, J. M. Calculating Polaron Mobility in Halide Perovskites. *arXiv:1704.05404 [cond-mat]* **2017** , arXiv: 1704.05404..
(29) Togo, A.; Chaput, L.; Tanaka, I. Distributions of Phonon Lifetimes in Brillouin Zones. *Phys. Rev. B: Condens. Matter Mater. Phys.* **2015**, *91*, 094306.
(30) Beecher, A. N.; Semonin, O. E.; Skelton, J. M.; Frost, J. M.; Terban, M. W.; Zhai, H.; Alatas, A.; Owen, J. S.; Walsh, A.; Billinge, S. J. L. Direct Observation of Dynamic Symmetry Breaking above Room Temperature in Methylammonium Lead Iodide Perovskite. *ACS Energy Lett.* **2016**, *1*, 880−887.
(31) Bertolotti, F.; Protesescu, L.; Kovalenko, M. V.; Yakunin, S.; Cervellino, A.; Billinge, S. J. L.; Terban, M. W.; Pedersen, J. S.; Masciocchi, N.; Guagliardi, A. Coherent Nanotwins and Dynamic Disorder in Cesium Lead Halide Perovskite Nanocrystals. *ACS Nano* **2017**, *11*, 3819−3831.
(32) Kovalsky, A.; Wang, L.; Marek, G. T.; Burda, C.; Dyck, J. S. Thermal Conductivity of $CH_3NH_3PbI_3$ and $CsPbI_3$: Measuring the Effect of the Methylammonium Ion on Phonon Scattering. *J. Phys. Chem. C* **2017**, *121*, 3228−3233.
(33) Klein, J. R.; Flender, O.; Scholz, M.; Oum, K.; Lenzer, T. Charge Carrier Dynamics of Methylammonium Lead Iodide: from PbI_2-Rich to Low-Dimensional Broadly Emitting Perovskites. *Phys. Chem. Chem. Phys.* **2016**, *18*, 10800−10808.
(34) Zhong, Y.; Ostach, D.; Scholz, M.; Epp, S. W.; Techert, S.; Schlichting, I.; Ullrich, J.; Krasniqi, F. S. Hot Carrier Relaxation in CdTe via PhononPlasmon Modes. *J. Phys.: Condens. Matter* **2017**, *29*, 095701.
(35) Rosenwaks, Y.; Hanna, M. C.; Levi, D. H.; Szmyd, D. M.; Ahrenkiel, R. K.; Nozik, A. J. Hot-Carrier Cooling in GaAs: Quantum Wells Versus Bulk. *Phys. Rev. B: Condens. Matter Mater. Phys.* **1993**, *48*, 14675−14678.
(36) Brivio, F.; Frost, J. M.; Skelton, J. M.; Jackson, A. J.; Weber, O. J.; Weller, M. T.; Goñi, A. R.; Leguy, A. M. A.; Barnes, P. R. F.; Walsh, A. Lattice Dynamics and Vibrational Spectra of the Orthorhombic, Tetragonal, and Cubic Phases of Methylammonium Lead Iodide. *Phys. Rev. B: Condens. Matter Mater. Phys.* **2015**, *92*, 144308.
(37) Wu, X; et al. Light-Induced Picosecond Rotational Disordering of the Inorganic Sublattice in Hybrid Perovskites. *Science Adv.* **2017**, *3*, e1602388.
(38) Miyata, K.; Meggiolaro, D.; Trinh, M. T.; Joshi, P. P.; Mosconi, E.; Jones, S. C.; De Angelis, F.; Zhu, X.-Y. Large Polarons in Lead Halide Perovskites. *Science Adv.* **2017**, *3*, e1701217.

DOI: 10.1021/acsenergylett.7b00862
ACS Energy Lett. 2017, 2, 2647−2652